Supplementary Materials

Dopamine restores reward prediction errors in old age

Rumana Chowdhury & Marc Guitart-Masip,
Christian Lambert, Peter Dayan, Quentin Huys,
Emrah Düzel, Raymond J Dolan

Supplementary Table 1. Older adults sample characteristics

32 older participants were recruited via advertisement in local public buildings, our departmental website and from a database of healthy volunteers held at King's College Hospital, London. Individuals were screened by telephone and excluded if they had any of the following: history of neurological, psychiatric or endocrinological disorders (including diabetes mellitus and thyroid dysfunction), metallic implants, tinnitus, major visual impairment, history of drug addiction. To control for vascular risk factors, individuals known to have had a stroke or transient ischemic attack, myocardial infarction or require more than one anti-hypertensive medication were not eligible for participation. All participants had a normal performance (within 1.5 SD of age-related norm) on a range of neuropsychological tests (Supplementary Table 1). All subjects had a normal neurological examination (performed by a neurologist R.C.) ensuring participants did not have concurrent undiagnosed neurological conditions. Participants in the current study (n = 32) were selected from a larger sample of 42 healthy older adults aged 65 – 75 years who had participated in a previous study in the preceding six months. Preselection was based on an assessment of magnetization transfer (MT) values of the SN/VTA where we investigated the effects of SN/VTA structural integrity on episodic memory. Full details of this have been published [1]. Briefly, 10 individuals with MT values of the SN/VTA scattered around the mean MT values of the group were excluded to increase the variance in the sample, resulting in 16 participants with higher MT values and 16 with lower MT values. Note that MT values of the SN/VTA remained normally distributed across the sample of 32 participants in the current study and MT did not correlate with any measures used in this study (behavioural, model parameters, functional parameter estimates or DTI metrics).

Age (yrs)	70.00 (3.24)
Gender M:F	11:21
Education (yrs)	16.28 (2.88)
National Adults Reading Test IQ	121.72 (6.36)
Body mass index	26.6 (4.40)
Non-smoker	31 (97%)
Normotensive	30 (94%)
Mini-Mental State Examination	30 (28-30)
Geriatric Depression Scale	1 (0-7)
Rey Auditory and Verbal Learning Test trials 1-5	50.2 (8.3)
Rey Auditory and Verbal Learning Test trial 7	9.5 (2.3)
D2 cancellation test of attention	152.3 (33.5)
Digit Span Forward	8 (4 – 9)
Digit Span Backward	5 (3 – 8)
Controlled Oral Word Association test phonemic fluency	58.0 (14.0)
Controlled Oral Word Association test semantic fluency	26.5 (6.6)
Visual and Object Space Perception number location	10 (8 - 10)

Demographic details and neuropsychological test scores are mean (SD), number (%) or median (range); n = 32

Supplementary Table 2. Model fitting, comparison and quality of the behavioural fits

All model-fitting procedures were verified on surrogate data generated from a known decision process. For Bayesian model comparison, we computed the model evidence, which was approximated in two steps. First, the integral over the hyperparameters was approximated via the Bayesian Information Criterion (BIC, which penalizes for model complexity) at the group level[2] using the integral over the individual parameters. This latter integral was approximated by sampling from the fitted priors. A pseudo-r^2 statistic was defined as (r – l)/r where l and r are the log likelihoods of the data under the model and under purely random choices respectively (P = .50 for all trials). We first compared the two full random effects models including one single alpha and beta term per participant or one single alpha and two beta terms (one per treatment condition) per participant (BIC one beta term: 12002; BIC two beta terms: 12001.6). As there was no evidence for a better fit when two separate betas (one per treatment session) were included, we proceeded by fitting the data with a learning model with beta fixed across the data ('single fixed beta') and the free parameters alpha (learning rate) and choice perseveration. The winning model as determined by the lowest BIC consisted of a single fixed beta, a learning rate alpha and a choice perseveration parameter. For completeness, we also repeated the fitting procedure with two fixed beta terms separately for placebo and L-DOPA ('two fixed betas'). This shows that adding the perseveration parameter also improved the model fit when two different betas for drug and placebo conditions were allowed.

	Single fixed beta		**Two fixed betas**	
	alpha	**alpha and perseveration**	**alpha**	**alpha and perseveration**
Pseudo-r^2	0.3707	0.3752	0.3662	0.3705
BIC	12498	12464	12592	12560

BIC: Bayesian information criterion

Supplementary Table 3. Individual differences in task performance, reinforcement learning and neural representations of reward and expected value

	Total won placebo	**Total won L-DOPA**
Model parameter		
alpha placebo	Rho = 0.39,p = .027*	-
alpha L-DOPA	-	Rho = 0.06, p = .727
fMRI parameter estimates		
$\boldsymbol{R(t)}$**placebo**	R = -0.07, p = .707	-
$\boldsymbol{Q_{a(t)}(t)}$ **placebo**	R = -0.42, p = .016*	-
$\boldsymbol{R(t)}$ **L-DOPA**	-	R = -0.21, p = .241
$\boldsymbol{Q_{a(t)}(t)}$ **L-DOPA**	-	R = -0.25, p = .171

*Correlations in older adults (n = 32) between task performance (total won) and learning rate (alpha) and functional parameter estimates of reward ($R(t)$) and expected value ($Q_{a(t)}(t)$). Rho = Spearman correlation; R = Pearson correlation; *p < 0.05 two-tailed*

Supplementary Table 4. Relationship between model likelihood and standard error of functional parameter estimates of reward and expected value

Group differences between the drug-induced change in the standard error of $\mathrm{R(t)}$ and $\mathrm{Q_{a(t)}(t)}$ and task performance were not a consequence of worse fits of the reinforcement learning models as the mean model likelihood was similar for all subgroups ('win less on L-DOPA' group on placebo 0.65; 'win less on L-DOPA' group on L-DOPA 0.65; 'win more on L-DOPA' group on placebo 0.64; 'win more on L-DOPA' group on L-DOPA 0.68). As shown in the table, there were no correlations either across participants between the mean model likelihood and the standard error of $\mathrm{R(t)}$ and the standard error of $\mathrm{Q_{a(t)}(t)}$.

	Win less on L-DOPA		**Win more on L-DOPA**	
	Placebo	**L-DOPA**	**Placebo**	**L-DOPA**
Standard error of $\mathbf{R(t)}$	Rho = -.09, p = .722	Rho = -0.12, p = .639	Rho = -0.21, p = .451	Rho = -0.03, p = .930
Standard error of $\mathbf{Q_{a(t)}(t)}$	Rho = 0.17, p = .510	Rho = 0.10, p = .694	Rho = -0.09, p = .761	Rho = 0.02, p = .950

$R(t)$: reward; $Q_{a(t)}(t)$: expected value; Rho = Spearman correlation

Supplementary Table 5. Physiological measures

Subjective mood ratings of how alert, content and calm participants felt were measured using Bond and Lader Visual Analogue Scales [3]. The lack of significant differences in how alert, content or calm participants rated themselves as feeling after receiving L-DOPA compared to placebo suggests participants were unaware of subtle physiological changes or the order of pharmacological manipulation. Heart rate was higher under L-DOPA than placebo and systolic blood pressure was lower under L-DOPA than placebo, though there was no difference in diastolic blood pressure. Importantly, adding systolic blood pressure and heart rate as covariates made no difference to the analysis of learning rate (L-DOPA vs. placebo, $F(1,28) = 6.95$, $p = .014$), no interaction between learning rate and heart rate ($p = .628$) or learning rate and blood pressure ($p = .831$)).

		t	**p**
	L-DOPA vs placebo, mean (SD)		
Alert	1.15 (9.26)	0.68	.502
Content	-2.26 (9.97)	-1.24	.224
Calm	0.30 (14.51)	0.11	.911
Heart Rate	3.53 (5.47)	3.65	.001
Systolic blood pressure	-8.26 (17.61)	-2.61	.014
Diastolic blood pressure	-2.94 (10.01)	-1.63	.113

Heart rate, blood pressure and subjective rating scales were recorded on arrival ('baseline') and after pharmacological manipulation immediately prior to performing the task ('task'), under placebo and L-DOPA. Changes from baseline to prior to performing the task ('task minus baseline') were compared between L-DOPA and placebo (paired t-tests, two-tailed). Mean (SD) difference measures indicate whether the measurement was lower under L-DOPA (negative number) or higher under L-DOPA (positive number).

Supplementary Table 6. Whole-brain fMRI results for the interaction between drug (L-DOPA > placebo) and reward prediction errors

	T	Z	x	y	z	L/R	Region
Reward							
	3.94	3.52	29	5	-20	R	sup temporal pole
	3.65	3.30	9	-45	27	R	post cingulum
	3.54	3.22	-48	-51	-23	L	inf temporal
	3.41	3.12	18	-1	0	R	thalamus
Expected value							
	3.96	3.54	-11	56	24	L	sup frontal
Putative reward prediction error							
	3.53	3.22	8	6	-3	R	caudate

'Putative reward prediction error' refers to the contrast reward > expected value. Results shown at the uncorrected threshold p < 0.001; no regions survived whole-brain FWE correction at the significance level p <0.05. N = 32

Supplementary Figure 1. Task performance in older adult subgroups

We performed a median split according to difference in performance (total won on L-DOPA minus total won on placebo) amongst older adults. This resulted in a group who 'win less on L-DOPA' (total won L-DOPA < placebo) and a group who 'win more on L-DOPA' (total won L-DOPA > placebo). Since the middle two participants had the same difference in performance, and this amount was negligible (+ £0.30), we included them in the 'win less on L-DOPA' group rather than 'win more on L-DOPA' group. This ensured that the 'win more on L-DOPA group provided a more robust representation of improved performance on L-DOPA. Consequently, the 'win less on L-DOPA group consisted of 17 participants (total won placebo: £13.12 (0.73); total won L-DOPA: £12.61 (0.57); paired t-test, $t(16) = -3.35$, $p = .004$) and the 'win more on L-DOPA' group consisted of 15 participants (total won placebo: £12.10 (0.75); total won L-DOPA: £13.31 (0.89); paired t-test, $t(14) = 6.68$, $p < 0.0005$).

The figure shows that performance under placebo was also not equivalent for the two groups and that the overall pattern of performance was consistent with an 'inverted U-shape'. A repeated measures ANOVA with total won (L-DOPA/placebo) as the within-subject factor and group (win less/win more) as the between-subject factor showed a performance* group interaction ($F(1,30) = 53.53$, $p < 0.0005$). Post hoc t-tests indentified that both baseline performance under placebo and performance on L-DOPA differed between groups (independent t-test 'win less on L-DOPA' vs. 'win more on L-DOPA' group: placebo, $t(30) = 3.91$, $p = <0.0005$; L-DOPA, $t(30) = -2.66$, $p = .012$). This was not an artefact of practice effects since the total won under L-DOPA and placebo did not interact with the order of drug administration (L-DOPA day 1/ L-DOPA day 2) (non-significant performance*order interaction: $F(1,30) = 0.20$, $p = .657$). In these subgroups, reaction time showed a weak trend towards being faster on L-DOPA than placebo in the 'win more on L-DOPA' group ($t(14) = -1.85$, $p = .085$), whereas there was no difference in the 'win less on L-DOPA' group ($t(16) = -0.09$, $p = .929$).

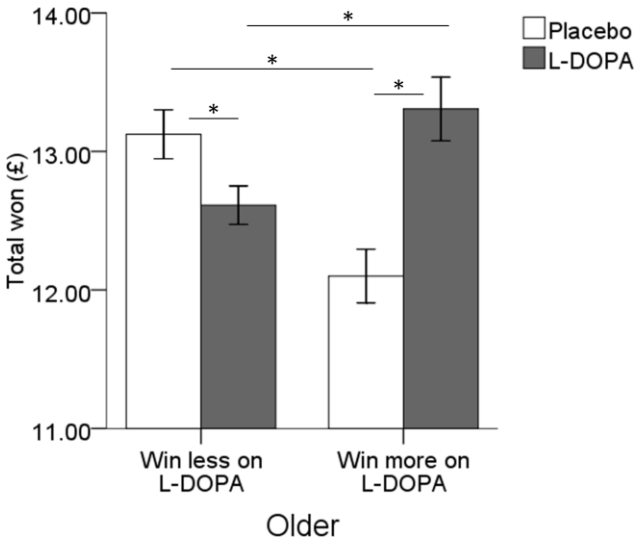

**p<0.05 two-tailed. Error bars are ±1 SEM. Win less on L-DOPA group (n = 17); win more on L-DOPA group (n = 15)*

Supplementary Figure 2. Steps taken to create the nucleus accumbens functional ROI

The borders of the nucleus accumbens cannot be clearly defined on routine MR imaging as there are no real intensity signatures at its boundaries, however the anatomical landmarks have been well described[4]. The Freesurfer package (version 4.5.0, http://surfer.nmr.mgh.harvard.edu/) includes a nucleus accumbens ROI that was derived from manually segmented subjects, based on the surrounding landmarks. To produce a concordant region across our study population, we used Freesurfer to obtain individual subject nucleus accumbens ROIs from the Freesurfer recon-all pipeline. Each subjects' nucleus accumbens mask was visually inspected to ensure accurate segmentation. The nucleus accumbens masks for each participant were warped to MNI space using DARTEL flowfields and averaged together to produce a binary mask at a threshold of 0.3. We defined fMRI brain regions at an uncorrected $p<0.001$ for the R > Q condition (reward > expected value; 'putative' reward prediction error), and then extracted the significant nucleus accumbens voxels using the thresholded binary nucleus accumbens mask to anatomically constrain the functional map, producing a functional ROI.

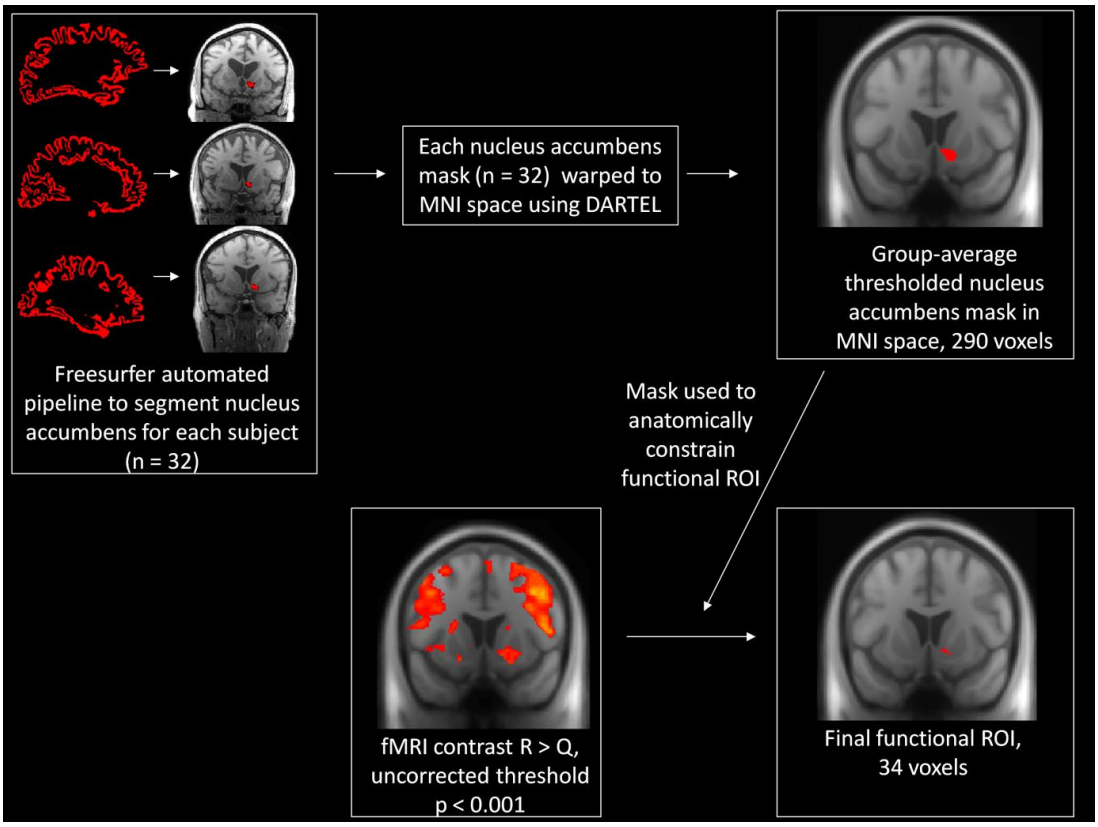

Supplementary Figure 3. Individual differences in standard error of functional parameter estimates and task performance

The drug-induced change (L-DOPA minus placebo) in the standard error of the parameter estimates of reward and expected value correlated negatively with the drug-induced change in the total amount won on the task in the 'win less on L-DOPA' group only. These correlations were significantly different between groups, measured using Fishers r-to-z transformation (reward, z = -2.00, p = .046 two-tailed; expected value, z = -2.26, p = .024 two-tailed).

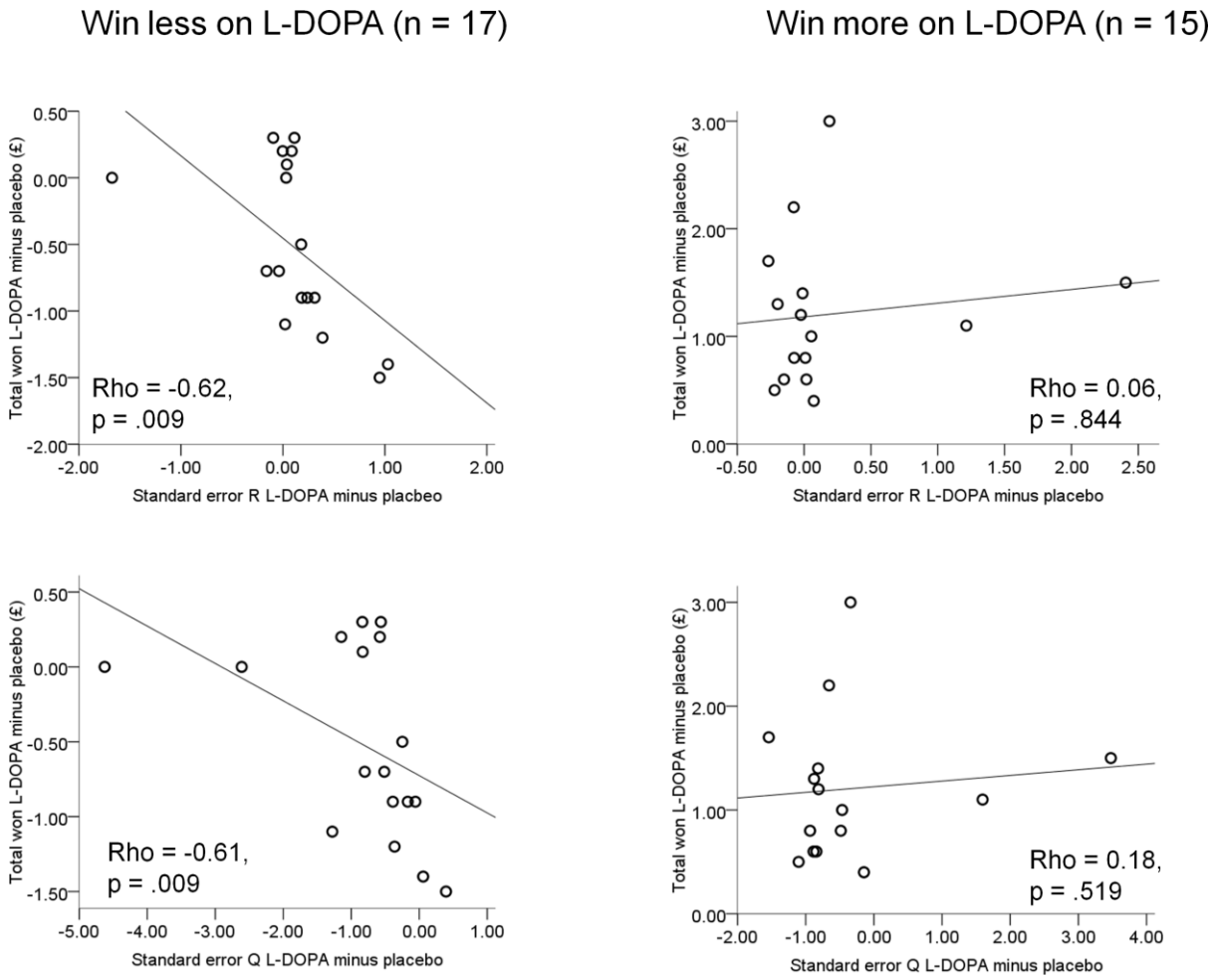

Rho = Spearman correlations (two-tailed).

Supplementary Figure 4. Relationship between expected value and task performance

Whole-brain multiple regression analyses identified a negative correlation between expected value and total won on the task in the left superior parietal cortex under placebo, and the left inferior parietal cortex and right precuneus under L-DOPA (FWE-p < 0.05; displayed at uncorrected threshold p < 0.001 on a group-average image; n = 32 older adults).

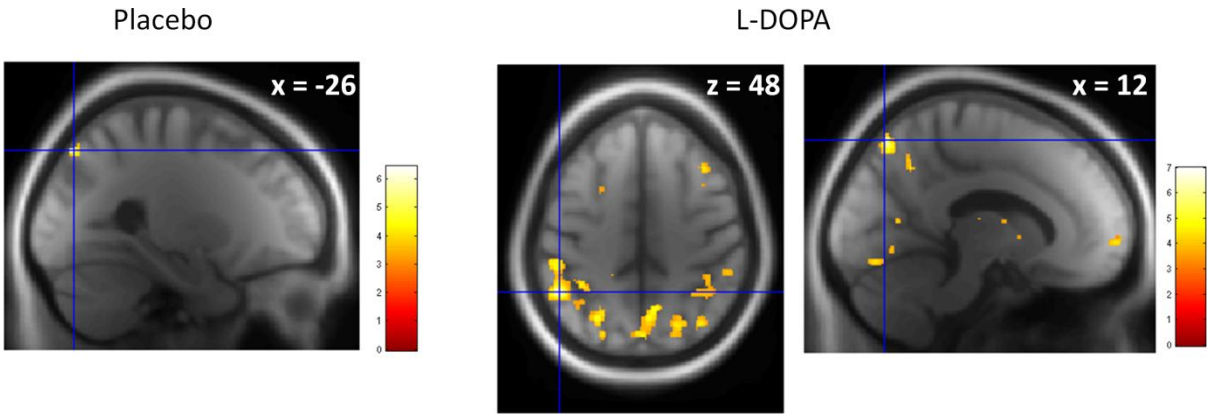

Supplementary Figure 5. Parameter estimates for reward and expected value on placebo

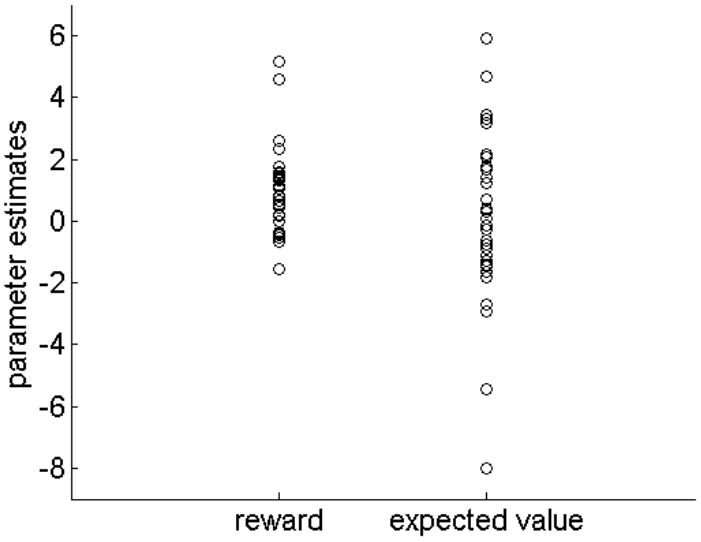

Each dot represents an older individual (n = 32)

Supplementary Figure 6. Diffusion tensor imaging connectivity strength maps

We used FSL version 4.1.4 and SPM8 for DTI preprocessing as follows: eddy current correction and correction for susceptibility artefacts[5], averaging of low b images to generate a brain mask for manual skull stripping, dtifit allowing fractional anisotropy to be calculated, BEDPOSTX, FNIRT (results manually checked for all individuals to ensure optimal alignment) and tractography using FSL's probtrackX software[6]. Each voxel was sampled 5000 times with a burn in of 1000, curvature threshold of 0.2, modelling two fibers per voxel, utilising the previously calculated warp fields.

Tractography was performed in each individuals' native space, from all voxels in each subject's anatomically-defined right SN/VTA ROI (seed: red ROI). We restricted our analysis to the right since this is where we determined our functional nucleus accumbens ROI. This SN/VTA was manually defined by R.C. on each subjects' MT-weighted image as per Düzel et al[7] using MRIcro [8]. Ten randomly selected SN/VTA ROIs were segmented by a second trained individual (C.L.) and showed high inter-rater reliability (Intraclass correlation = 0.87, $p<0.0005$). The single target mask of the right striatum (target: green ROI) was defined using the caudate and putamen masks from the AAL toolbox[9]. This MNI-space mask was normalised to each individuals' native space using the inverse of the normalisation parameters. To avoid erroneous tractography results, we created individual subject exclusion masks using ITK-SNAP[10]. The ventricles and CSF spaces were automatically defined using the "snake" function, and particular attention was paid to manually refine the region surrounding the cerebral peduncle and medial wall of the temporal lobe.

We generated 'relative connectivity strength' maps using the following steps. Here the probabilistic index of connectivity (PICo) between a seed and any other voxel in the brain is given by the number of traces arriving at the target site and is equivalent to the term "samples" used by other authors[11]. **Step 1: Generate individual seed voxel PICo maps for every seed voxel.** In each map, the voxel values represents the number of samples (from 0 - 5000) originating from the seed passing through a voxel, using probtrackX. **Step 2: Generate individual ROI probability maps.** We calculated the maximum PICo value that occurred within the ROI of interest across all seed PICo maps, then thresholded the individual seed PICo maps at 0.02% of the maximum ROI PICo value [12]. The individual seed maps were combined so that the value at each ROI voxel then becomes the maximum PICo for that voxel across every seed map. **Step 3: Generate "Relative Connectivity Strength" maps**. The ROI probability maps were divided by the sum of all PICo values within that specific map.

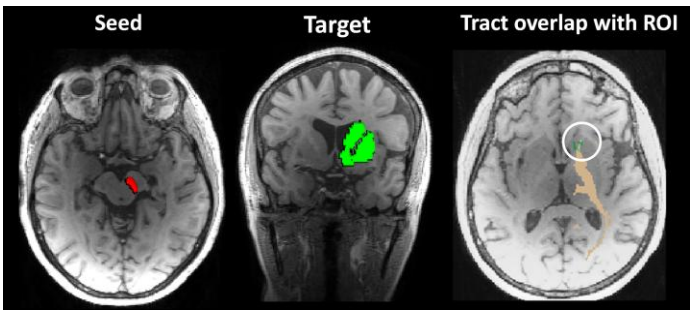

Single subject example of probabilistic tractography (gold = tract) from a seed in the right substantia nigra/ventral tegmental area (red) to the striatum target (green) which overlapped with the functional nucleus accumbens ROI (circled).

Supplementary Figure 7. Individual differences in DTI connectivity strength and expected value representations in older adult subgroups

Both older participants who won less on L-DOPA than placebo and older participants who won more on L-DOPA than placebo showed a negative association between anatomical nigro-striatal connectivity strength and functional parameter estimates of expected value in nucleus accumbens ('win less on L-DOPA': Rho = -0.37, p = .154; 'win more on L-DOPA': Rho = -0.54, p = .047).

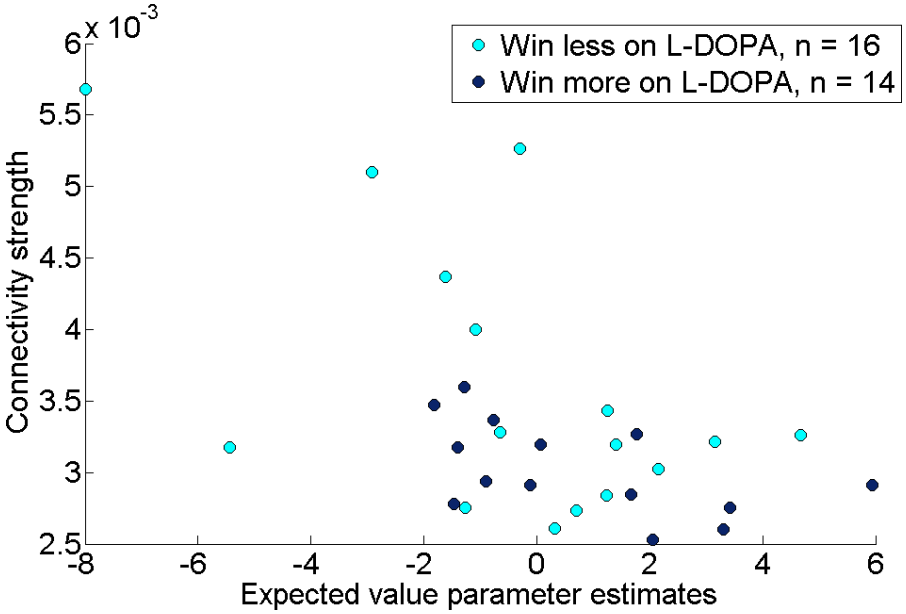

References

1. Chowdhury, R., Guitart-Masip, M., Bunzeck, N., Dolan, R.J. & Duzel, E. Dopamine Modulates Episodic Memory Persistence in Old Age. *The Journal of Neuroscience* **32**, 14193-14204 (2012).
2. Kass, R. & Raftery, A. Bayes factors. *Journal of the American Statistical Association* **90** (1995).
3. Bond, A. & Lader, M. The use of analogue scales in rating subjective feelings. *British Journal of Medical Psychology* **47**, 211-218 (1974).
4. Neto, L.L., Oliveira, E., Correia, F. & Ferreira, A.G. The Human Nucleus Accumbens: Where Is It? A Stereotactic, Anatomical and Magnetic Resonance Imaging Study. *Neuromodulation: Technology at the Neural Interface* **11**, 13-22 (2008).
5. Andersson, J.L.R., Skare, S. & Ashburner, J. How to correct susceptibility distortions in spin-echo echo-planar images: application to diffusion tensor imaging. *Neuroimage* **20**, 870-888 (2003).
6. Behrens, T.E.J., Berg, H.J., Jbabdi, S., Rushworth, M.F.S. & Woolrich, M.W. Probabilistic diffusion tractography with multiple fibre orientations: What can we gain? *Neuroimage* **34**, 144-155 (2007).
7. Düzel, S.*, et al.* A close relationship between verbal memory and SN/VTA integrity in young and older adults. *Neuropsychologia* **46**, 3042-3052 (2008).
8. Rorden C, B.M. Stereotaxic display of brain lesions. *Behavioral Neurology* **12**, 191-200 (2000).
9. Brett, M., Anton, J.-L., Valabregue, R., and Poline, J.-B. Region of interest analysis using an SPM toolbox. *8th International Conference on Functional Mapping of the Human Brain (Sendai, Japan)* (2002).
10. Yushkevich, P.A.*, et al.* User-guided 3D active contour segmentation of anatomical structures: Significantly improved efficiency and reliability. *Neuroimage* **31**, 1116-1128 (2006).
11. Forstmann, B.U.*, et al.* The Speed-Accuracy Tradeoff in the Elderly Brain: A Structural Model-Based Approach. *The Journal of Neuroscience* **31**, 17242-17249 (2011).
12. Aron, A.R., Behrens, T.E., Smith, S., Frank, M.J. & Poldrack, R.A. Triangulating a Cognitive Control Network Using Diffusion-Weighted Magnetic Resonance Imaging (MRI) and Functional MRI. *The Journal of Neuroscience* **27**, 3743-3752 (2007).